PHILOSOPHICAL TRANSACTIONS B

rstb.royalsocietypublishing.org

Research

Cite this article: Lawrence EA, Kague E, Aggleton JA, Harniman RL, Roddy KA, Hammond CL. 2018 The mechanical impact of *col11a2* loss on joints; *col11a2* mutant zebrafish show changes to joint development and function, which leads to early-onset osteoarthritis. *Phil. Trans. R. Soc. B* **373**: 20170335.
http://dx.doi.org/10.1098/rstb.2017.0335

Accepted: 3 July 2018

One contribution of 14 to a Theo Murphy meeting issue 'Mechanics of development'.

Subject Areas:
biomechanics, developmental biology, genetics, molecular biology

Keywords:
zebrafish, biomechanics, collagen, cartilage, Stickler syndrome, development

Author for correspondence:
Chrissy L. Hammond
e-mail: chrissy.hammond@bristol.ac.uk

The mechanical impact of *col11a2* loss on joints; *col11a2* mutant zebrafish show changes to joint development and function, which leads to early-onset osteoarthritis

Elizabeth A. Lawrence[1,†], Erika Kague[1,†], Jessye A. Aggleton[2], Robert L. Harniman[3], Karen A. Roddy[1] and Chrissy L. Hammond[1]

[1]School of Physiology, Pharmacology and Neuroscience, University of Bristol, Bristol BS8 1TD, UK
[2]School of Anthropology and Archaeology, University of Bristol, Bristol BS8 1UU, UK
[3]School of Chemistry, University of Bristol, Bristol BS8 1TS, UK

EK, 0000-0002-0266-9424; JAA, 0000-0002-9765-3758; CLH, 0000-0002-4935-6724

Collagen is the major structural component of cartilage, and mutations in the genes encoding type XI collagen are associated with severe skeletal dysplasias (fibrochondrogenesis and Stickler syndrome) and early-onset osteoarthritis (OA). The impact of the lack of type XI collagen on cell behaviour and mechanical performance during skeleton development is unknown. We studied a zebrafish mutant for *col11a2* and evaluated cartilage, bone development and mechanical properties to address this. We show that in *col11a2* mutants, type II collagen is made but is prematurely degraded in maturing cartilage and ectopically expressed in the joint. These changes are correlated with increased stiffness of both bone and cartilage; quantified using atomic force microscopy. In the mutants, the skeletal rudiment terminal region in the jaw joint is broader and the interzone smaller. These differences in shape and material properties impact on joint function and mechanical performance, which we modelled using finite element analyses. Finally, we show that *col11a2* heterozygous carriers reach adulthood but show signs of severe early-onset OA. Taken together, our data demonstrate a key role for type XI collagen in maintaining the properties of cartilage matrix; which when lost leads to alterations to cell behaviour that give rise to joint pathologies.

This article is part of the Theo Murphy meeting issue 'Mechanics of development'.

1. Introduction

Articular cartilage is a highly specialized connective tissue, which provides a smooth, lubricated surface for articulation and load transmission with low joint friction. Collagen is a major constituent of cartilage, accounting for around 75% of its dry weight [1]. Type II collagen makes up 90–95% of the collagen network, while the remaining 5–10% comprises other collagens such as type IX and XI, with studies of chick articular cartilage showing association of these three collagen types in a tight D-periodic array [2,3]. These minor collagens help to organize and stabilize the type II collagen fibril network that, along with proteoglycans, water and other proteins, form a dense extracellular matrix (ECM) in which chondrocytes are dispersed [4]. The tight fibrillar structure from collagens and the water content, from interaction with glycosaminoglycans (GAGs), govern the mechanical properties of the cartilage.

[†]These authors contributed equally to this study.

Electronic supplementary material is available online at http://dx.doi.org/10.6084/m9.figshare.c.4195418.

THE ROYAL SOCIETY PUBLISHING

Type XI collagen belongs to the fibril-forming class of collagens; it is formed as a heterotrimer of three chains, each encoded by a different gene: *COL11A1* [5], *COL11A2* and *COL2A1* [6,7]. While the α1 chain of type XI collagen is expressed in both cartilaginous and ocular tissue, the α2 chain is predominantly expressed in cartilage.

Given the close interaction between type II and type XI collagens, mutations that affect either can cause similar destabilization of cartilage organization, as observed in Marshall Stickler syndrome. Stickler syndrome, which affects around 1 in 7500 new-borns, encompasses a hereditary group of conditions caused by defective type II, IX or XI collagen [8] and is divided in to three phenotypes: depending on the collagen mutation present. Type III is associated with mutations to the type XI gene *COL11A2* [9,10]. Type III Stickler syndrome is characterized by skeletal, orofacial and auditory abnormalities including: scoliosis, hearing loss, cleft palate, joint hypermobility [11], multiple hereditary exostoses [10] and premature osteoarthritis (OA) in 75% of patients before the age of 30 [8]. The majority of mutations linked to Stickler syndrome lead to truncated proteins lacking the c-terminal domain of the peptide, disturbing the association of the α helices to form procollagens and consequentially the formation of collagen fibrils and fibres [12]. Mutations in genes encoding type XI collagens are also associated with other skeletal dysplasias, including the severe developmental condition fibrochondrogenesis [13], and Weissenbacher–Zymuller syndrome [9].

Mutant mice for *Col11a1* (*Cho*$-/-$) are neonatally lethal and show decreased limb bone length, cleft palate and short snouts [14], and thicker, less uniform collagen fibrils in the cartilage ECM [15]. Type II collagen degradation [16] and early-onset OA were reported in *Cho*/+ heterozygous mice [17]. Additionally, mice haploinsufficient for *Col11a1* display altered susceptibility to load-induced damage [18]. While *Col11a2* mutant mice have been reported to show hearing loss, their skeletal phenotype has not been described [19]. The interaction of type XI collagen with type II is important for the maintenance of the spacing and diameter of type II collagen fibrils [20]. As type II collagen is the major collagen in cartilage, changes to its organization can impact the mechanical performance of the cartilage. Computational modelling has shown that spacing and interconnectivity between collagen fibrils has a significant effect on the mechanical performance of cartilage [21]. Cartilage is an intrinsically mechanically sensitive tissue, and changes to cartilage biomechanical performance have been extensively described during development [22], ageing and disease [23]. It is also increasingly well understood that subtle changes to skeletal morphology and joint shape can increase susceptibility to joint conditions such as OA later in life [24]. A recent large genome-wide association study on hip shape identified *COL11A1* as a contributor to hip shape [25]. Joint shapes seen in development and disease have been shown to have significant impact on the biomechanical performance of joints [24,26]. What is less clear is the sequence of events within the joint, do changes to shape precede changes to cartilage structure and mechanical performance or vice versa, and what is the relative impact of each change?

Zebrafish are an attractive model for studying the effect of genetic lesions on skeletal development. The larvae are translucent which, twinned with fluorescent reporter transgenic lines, enables dynamic imaging of skeletal cells [27,28] and the development of the zebrafish craniofacial skeleton is well documented [29–31]. The zebrafish jaw joint is synovial [32] and requires mechanical input to form normally [33,34]. Acute knockdown of *col11a1* in zebrafish using morpholinos has been shown to affect chondrocyte maturation [35], but no stable mutants for *col11a1* or *col11a2* have previously been reported.

Here, we show that larval zebrafish carrying a *col11a2* mutation display a variety of phenotypes including alterations to: joint shape, cartilage composition, cell organization and the material properties of the cartilage during development. These changes impact on the biomechanical and functional performance of the joint. The mutant fish go on to display phenotypes consistent with Stickler syndrome such as altered face shape and early-onset OA. Taken together, these data suggest that mechanical and cellular changes to the developing skeleton explain the predisposition of people with mutations in type XI collagens to early-onset OA.

2. Methods

(a) Zebrafish husbandry and transgenic lines

Zebrafish were maintained as described previously [36], all experiments were approved by the local ethics committee and performed under a UK Home Office Project Licence. Transgenic lines *Tg(col2a1aBAC:mcherry)*, *Tg(col10a1aBAC:citrine)hu7050* [37] and *Tg(smyhc1:GFP)* [38] have been described previously. *col11a2*^{sa18324} mutant zebrafish was generated by the Zebrafish Mutation Project (Sanger Institute) and acquired from the European Zebrafish Resource Centre (EZRC). It carries a non-sense mutation (C > A base pair change at position 228aa, zv9 chr19: 7834334), leading to a premature stop codon which shortens the polypeptide to about one-third of the triple helical domain of the α2 chain of collagen XI.

(b) DNA extraction and genotyping

Fins were clipped from anaesthetized or fixed zebrafish and incubated in base solution (25 mM NaOH,0.2 mM EDTA) before the addition of neutralization solution (40 mM Tris–HCl, pH 5.0). For genotyping, we used KASP (LGC) genotyping or PCR followed by Sanger sequencing (*col11a2* F-GGTGGCCTGATTCT GACCA; *col11a2* R-TATCTCACACCAGGATGCCG). Mutants were identified by C > A base pair change at position 228aa.

(c) Wholemount immunohistochemistry

Performed as previously described [37]. Primary antibodies and dilutions used were: rabbit pAb to collagen II, (*abcam* ab34712), 1 : 500; mouse pAb to collagen II, (*DHSB* II-II6B3), 1 : 500, rabbit pAb to collagen I, (*abcam* ab23730), 1 : 100. Secondary antibodies were Dylight 488 or 550 (*Thermo Scientific*) used at a dilution of 1 : 500. For imaging, larvae were mounted ventrally in 1% agarose and imaged on a Leica SP5 confocal microscope with a 10× objective.

(d) Three dimensions render generation, joint measurements, quantification of exostoses and cell circularity

Three-dimensional (3D) volume renders, surface models and measurements were acquired using Amira 6.0 (FEI). Surface models were generated manually by segmenting jaw joints using the segmentation tool. Measurements, as depicted in figures 1*c*,*d* and 3*a*, were taken using the 3D perspective

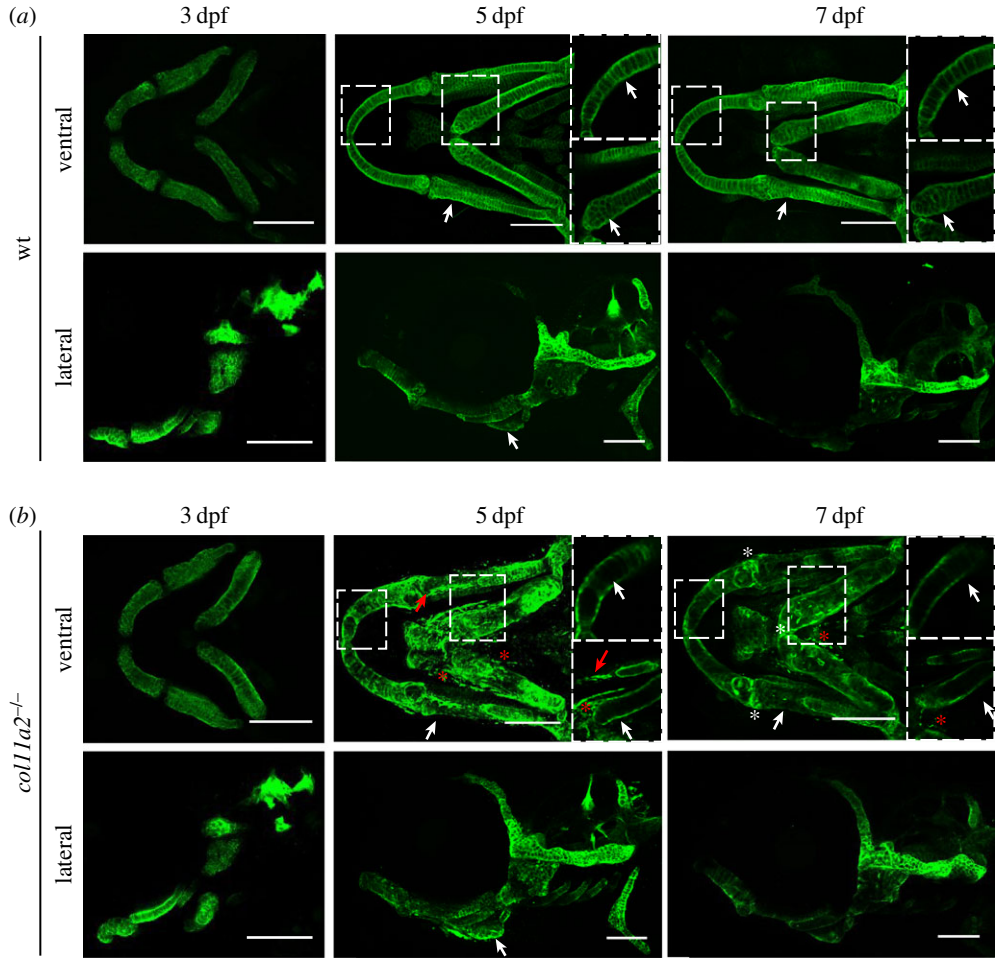

Figure 1. *col11a2* zebrafish mutant larvae show progressively altered type II collagen protein localization in jaw cartilage. (*a*,*b*) Maximum projection of ventral and lateral confocal image stacks from wt (*a*) and homozygous mutant (*col11a2*−/−) (*b*) larvae immunostained for type II collagen at three time points (3, 5 and 7 dpf). White arrows indicate areas of change in type II collagen distribution in the ECM. Dashed insets show single-stack images of regions with reduced deposition (white asterisks represent areas where type II collagen is maintained in mutant fish and red asterisks show fragments of type II collagen-positive material outside the main cartilage elements). Red arrows show interoperculomandibular (IOM) ligament. Scale bar, 100 µm.

measurement tool. To better visualize exostoses, 3D volume renders were created, and the greyscale range of colour applied. Exostoses were quantified in each lower-jaw element from single confocal image stacks in ImageJ [39] using the multi-point tool. Cell circularity was measured from confocal image stacks of type II collagen immunostained zebrafish larvae at 5 dpf. The freehand selection tool in ImageJ was used to outline chondrocytes in three distinct jaw regions (shown in figure 2*h*) and the measure function was used to analyse the circularity of each cell. This was done for 10 cells in each region, in 3 wild-type (wt) and 3 *col11a2* mutant zebrafish.

(e) Live imaging of transgenic fish

Live larvae at 5 dpf were anaesthetized in 0.1 mg ml^{-1} MS222 and mounted ventrally in 0.3% agarose with tricaine prior to being imaged on a Leica SP5II confocal microscope with a 10× objective. The number of slow muscle fibres and *col10a1a*-expressing cells were quantified manually in ImageJ from confocal images of double transgenic *Tg(smyhc1:GFP);(Col2a1aBAC:mCherry)* and *Tg(col10a1aBAC:citrine); (col2a1aBAC:mCherry)* zebrafish at 5 dpf, respectively.

(f) Alcian blue and alizarin red staining

The 5 and 7 dpf wt and *col11a2* mutant larvae were stained following a previously described protocol [40] and imaged on a Leica MZ10F stereo microscope prior to genotyping.

(g) *In situ* hybridization

In situ hybridization was performed as described [41] using a previously described *col11a2* probe [42]. Larvae were imaged on GXM-L3200 B upright microscope.

(h) Nanoscale surface morphology and Young's moduli

Atomic force microscopy (AFM) was performed on adult (1 year) bone and larval (7 dpf) cartilage from wt and *col11a2* mutant fish. A multi-mode VIII AFM with Nanoscope V controller and PeakForce control mechanism were used and the force-curves measured for means of set-point control in the PeakForce system and analysed in real time to provide quantitative nanomechanical mapping (QNM) of the samples. QNM analysis was conducted with both Nusense SCOUT cantilevers (NuNano, Bristol, UK) (nominal tip radius 5 nm, spring constants 21–42 N m^{-1}) and RTESPA-300 cantilevers (Bruker, CA, USA) (nominal tip radius 8 nm and spring constants 30–60 N m^{-1}), while high-resolution imaging of topographic features was conducted using SCANASYST-AIR-HR cantilevers (Bruker) (nominal tip radius of 2 nm). The system was calibrated for measurement of Young's modulus (YM) fitting with DMT models, using the relative method and samples of known YM (highly oriented pyrolytic graphite (18 GPa) and PDMS-SOFT-1-12M (2.5 MPa) (Bruker)), for bone and cartilage measurements, respectively. Bone was investigated in ambient environment while cartilage was maintained in a hydrated state post-dissection to minimize structural changes from drying. A root-mean-square mean was calculated for 65 536

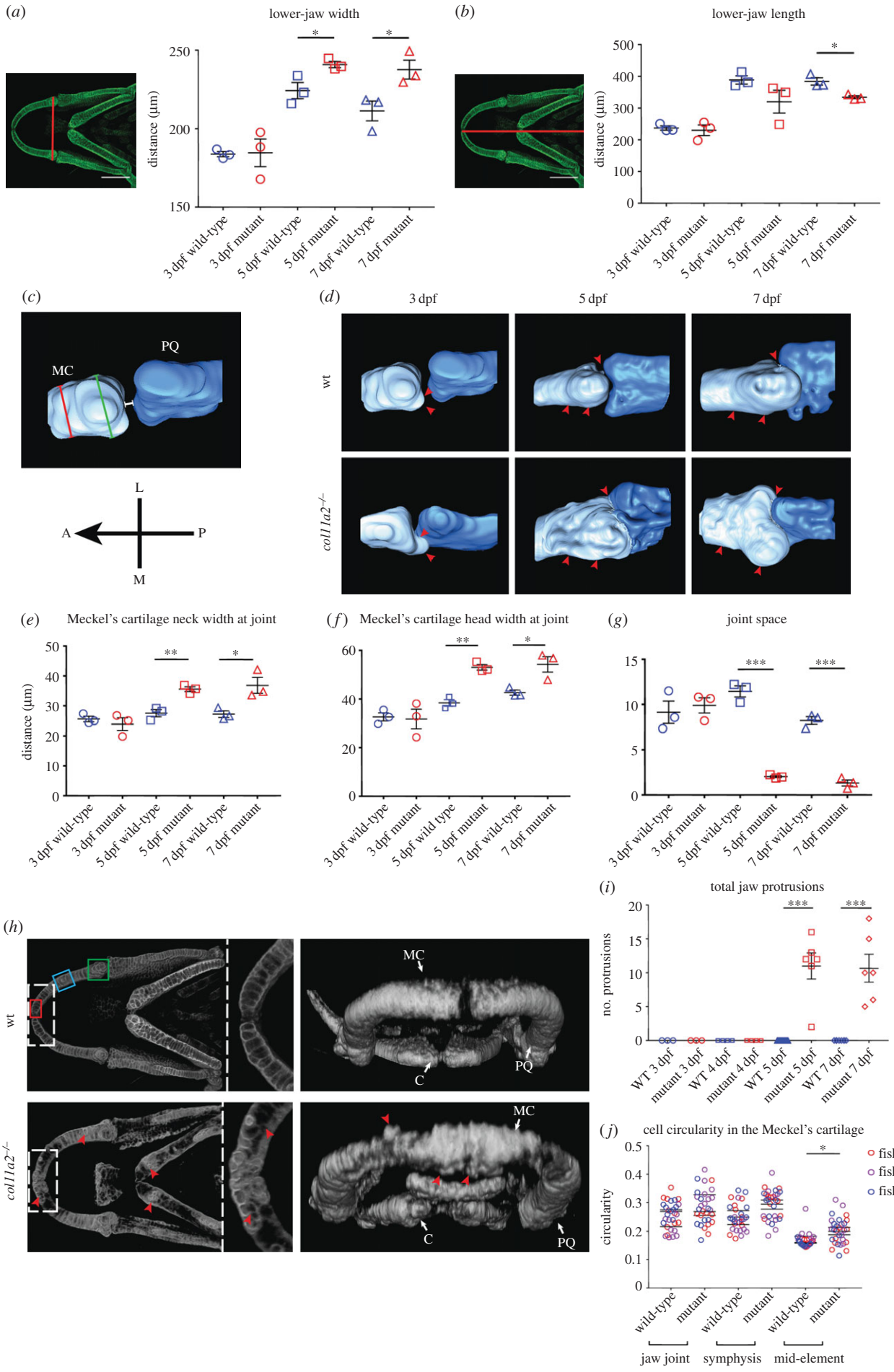

Figure 2. (*Caption opposite.*)

Figure 2. (*Opposite*). *col11a2* mutant zebrafish develop altered morphology and joint spacing in the lower jaw. (*a*,*b*) Lower-jaw shape quantification ($n = 3$ for all), location of measurements shown to the left of graphs. (*c*) Representation of measurements taken of joint neck (red line), joint head (green line) and joint space (white line) (Meckel's cartilage, light blue; palatoquadrate, dark blue). Orientation compass: A, anterior; L, lateral; M, medial; P, posterior. (*d*) Three-dimensional surface renders of jaw joint from confocal images of wt and *col11a2*−/− at 3, 5 and 7 dpf. Red arrowheads, areas of change. (*e*–*g*) Quantification of joint morphology at the Meckel's cartilage neck at joint (*e*), Meckel's cartilage head at joint (*f*) and joint space (*g*) ($n = 3$ for all). (*h*) Three-dimensional volume renders of wt and *col11a2*−/− zebrafish at 7 dpf. Dashed insets show Meckel's symphysis at higher magnification (red arrowheads, protruding cells). (*i*) Quantification of protruding cells in wt and *col11a2*−/− zebrafish at 3–7 dpf ($n = 3, 3, 4, 4, 13, 6, 8, 6$). (*j*) Quantification of cell circularity in the Meckel's cartilage in 5 dpf wt and *col11a2*−/− fish ($n = 3$ for all). Location of measurements shown in *h* (red box, Meckel's symphysis; blue box, mid-element; green box, jaw joint). Student's unpaired *t*-tests performed in *a*, *b*, *e*–*g*, *i* and *j*: data are mean with SEM (*j* shows mean with no SEM, *t*-tests performed between mean values). $*p \leq 0.05$, $**p \leq 0.01$, $***p \leq 0.001$.

measurements taken over a 500 × 500 nm region, three repeats were performed per sample; repeated on three fish per genotype.

(i) Finite element models

Single specimens that were representative of the confocal *z*-stacks of 7 dpf wt or mutant larvae dataset and their relative morphology were selected for the meshes. Cartilage elements were segmented in Scan IP using Otsu segmentation (electronic supplementary material, figure S2*a*), then a solid geometry created using the interpolation and 3D wrap tool. Smoothing filters (recursive Gaussian at 1px3) were used on the meshes to blend any rough small element clusters.

Cartilage geometry close to the joint was separated from the main cartilage in a duplicate mesh using the 3D editing tool allowing us to assign different material properties to hypertrophic chondrocytes and immature chondrocytes (electronic supplementary material, figure S2*b*). The mesh of the cartilage near the joints was subtracted from the original cartilage mesh using a Boolean operation. The meshes were added to a model and each part assigned their respective elastic isotropic material properties based on AFM measurements; values in electronic supplementary material, figure S2 and table S1.

The models were imported into Abaqus and two steps created: one to simulate jaw closure and two for jaw opening. Boundary conditions were applied to these steps, with the jaw constrained in all axes of motion at the ceratohyal to anchor it in space, and in *y* and *z* at the base of the palatoquadrate. Muscle forces, direction of opening/closure and muscle attachment points were as previously described [43]. The datum tool in Abaqus was used to create a custom rectangular datum coordinate system for each muscle; then used as the coordinate system for force direction between each muscle's insertion and origin to ensure force travelled along the same vector from one end to the other. A job was created and executed for the model, and the output analysed for stress, strain and displacement.

(j) Measurement of jaw displacement and movement frequency

High-speed movies were made of jaw movements in wt and *col11a2* mutants; frames corresponding to maximum jaw displacements were selected, imported into ImageJ and the difference, in micrometre, between resting and open states at points shown in figure 5*a* recorded. The number of mouth movements in 1000 frames was recorded from 7 wt and 7 *col11a2* mutant fish as previously described in [30].

(k) Micro-computed tomography

Three *col11a2* +/− and 3 wt adult fish of the same age (1-year-old) were fixed in 4% PFA for one week followed by sequential dehydration to 70% ethanol. Heads were scanned using an XT H 225ST micro-computed tomography (CT) scanner (Nikon) with a voxel size of 5 µm, X-ray source of 130 kV, 53 µA and without additional filters. Images were reconstructed using CT Pro 3D software (Nikon).

(l) Histology

Three 1-year-old *col11a2* +/− and 3 wts were decalcified in 1 M EDTA solution for 20 days. Samples were dehydrated in ethanol, embedded in paraffin and sagittally sectioned at 8 µm, relevant joint sections were de-waxed and stained with 1% Alcian blue 8GX (pH 2.5), then counterstained with haematoxylin and eosin. We adapted the OARSI cartilage OA histopathology grading system [44] to grade severity of OA. Five sections per jaw joint (per fish $n = 3$ fish) were scored. PicroSirius red staining was performed using 0.1% Sirius red F3B in saturated aqueous Picric acid, washed in acidified water, dehydrated and mounted under coverslips with DPX, then imaged using polarizing filters.

(m) Second harmonic generation

Second harmonic generation (SHG) images were acquired from histological sections of wt and *col11a2* +/− ($n = 3$ fish for each genotype) using 25x 0.3 NA water dipping lens, 880 nm laser excitation and simultaneous forward and backward detection (440/20) in Leica SP8 AOBS confocal laser scanning microscope attached to a Leica DM6000 upright epifluorescence microscope with multiphoton lasers and confocal lasers allowing fluorescent and SHG acquisition of the same sample and *z*-stack. Microscope parameters for SHG acquisition were set as described previously [45]. Maximum projection pictures were assembled using LAS AF Lite software (Leica).

3. Results

(a) *col11a2* and *col2a1* are co-expressed in the zebrafish lower jaw

To establish the extent of *col11a2* expression in cartilage, we performed *in situ* hybridization in larval zebrafish. Strong *col11a2* expression could be seen throughout the craniofacial cartilages including the Meckel's cartilage, palatoquadrate, ceratohyal and ethmoid plate (electronic supplementary material, figure S1*a*). At 3 dpf, the expression pattern of *col11a2* largely overlapped the expression of the type II collagen gene *col2a1a* visualized with the *Tg(col2a1aBAC:mCherry)* reporter zebrafish (electronic supplementary material, figure S1*b*). The domain of *col11a2* expression labelled more of the joint than was labelled by the *col2a1a* transgene, and expression of both *col11a2* and *col2a1a* preceded that of the mature type II protein, visualized by immunostaining, such that immature cells at the jaw joint and Meckel's symphysis express *col11a2* and *col2a1a* RNA at 3 dpf but not the mature type II protein (electronic supplementary material, figure S1*c*).

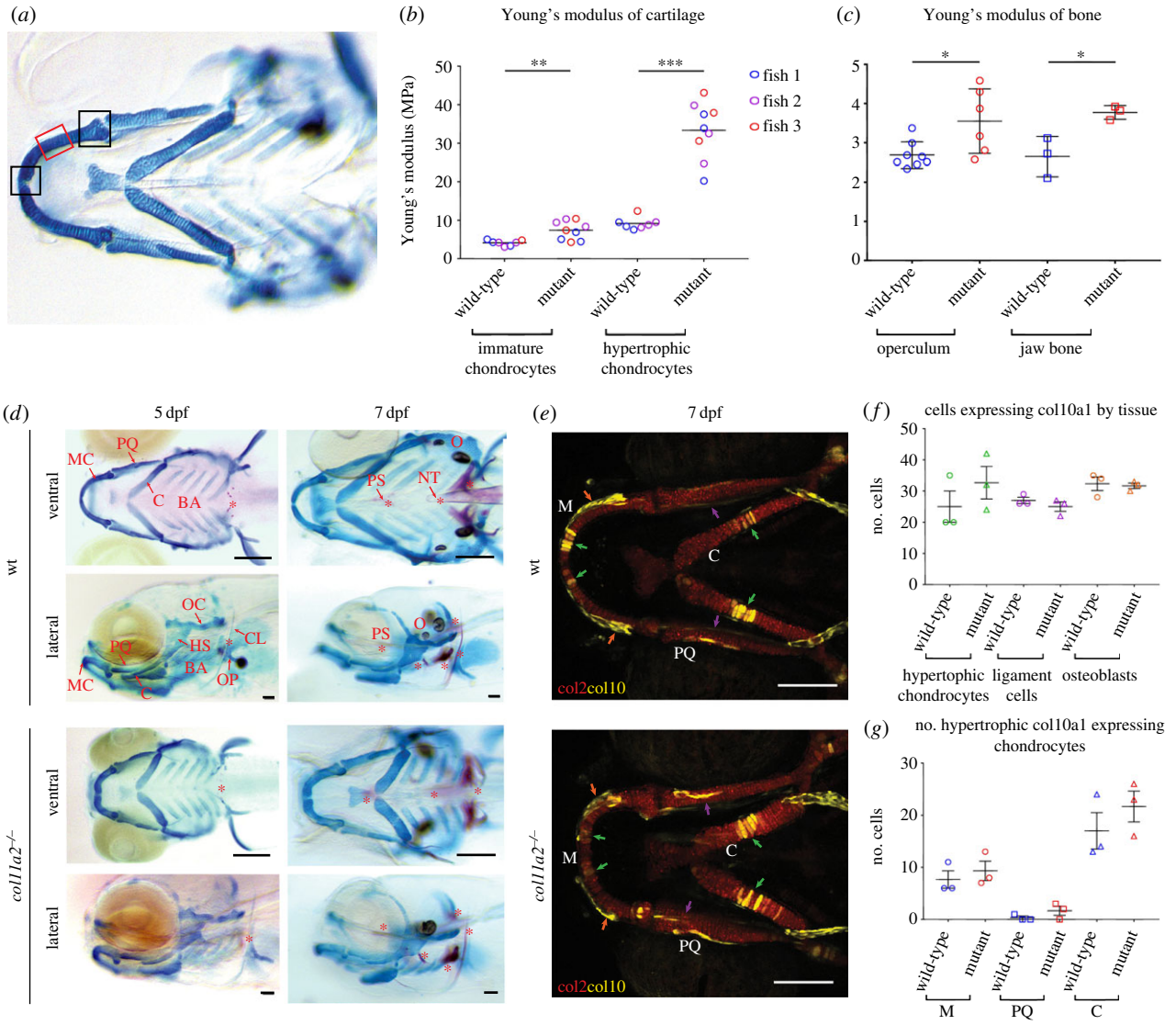

Figure 3. *col11a2* mutants have altered material properties in more mature cartilage which is not explained by increased mineralization or hypertrophy. Location of AFM measurements taken from larvae shown in (*a*). Measurements for immature chondrocytes taken from either of the two areas marked by black boxes, measurements for hypertrophic chondrocytes taken from area marked by red box. (*b*,*c*) YM values for (*b*) immature and hypertrophic chondrocytes in wt and *col11a2*−/− ($n = 3$ for both) at 7 dpf and (*c*) adult bone from the operculum and jaw in wt ($n = 8$ and 3, respectively) and *col11a2*−/− ($n = 6$ and 3, respectively). (*d*) Ventral and lateral views of Alizarin red Alcian blue staining show GAGs in cartilage (stained in blue) and mineralization (stained in red) in wt and *col11a2*−/− fish at 5 and 7 dpf. Red asterisks indicate areas of bone formation. MC, Meckel's cartilage; PQ, palatoquadrate; C, ceratohyal; BA, branchial arches; HS, hyosymplectic; OC, otic capsule; OP, operculum; CL, cleithrum; PS, parasphenoid; NT, notochord tip; O, otoliths. Scale bar, 200 µm. (*e*) *col10a1aBAC:citrine;col2:mCherry* transgenic line shows type X (yellow) and type II (red) collagen in wt and *col11a2*−/− zebrafish at 7 dpf. Scale bar, 100 µm. (*f*) Quantification of *col10a1*-expressing cells in hypertrophic chondrocytes, IOM ligament cells and osteoblasts in the lower jaw at 7 dpf (position of each cell type shown by green, purple and orange arrows in (*e*), respectively) ($n = 3$ for all). (*g*) Quantification of *col10a1*-expressing hypertrophic chondrocytes in 7 dpf wt and *col11a2*−/− fish ($n = 3$ for all) (M, Meckel's cartilage; PQ, palatoquadrate; C, ceratohyal). Student's unpaired *t*-tests were performed in *b*, *c*, *f* and *g*, data are mean with s.e.m. (*b* shows mean with no s.e.m.). $*p \leq 0.05$, $**p \leq 0.01$, $***p \leq 0.001$.

(b) *Col11a2* mutants show atypical type II collagen localization as they develop

As type XI collagen has previously been reported in the core of type II collagen fibrils [3] and is thought to have a role in the stability of type II collagen [46], we wanted to test whether loss of *col11a2* in zebrafish would impact type II collagen stability. For this, we studied the *col11a2* ^{sa18324} mutant which carries a non-sense mutation that introduces a premature stop codon at amino acid 228 (of 1877). We observed non-sense-mediated decay in mutants *in situ* hybridized for the *col11a2* probe (data not shown); therefore, it represents a null mutant. This mutant was crossed with the Tg(*col2a1a:mCherry)* to visualize expression of *col2a1a* and we studied its expression in craniofacial cartilages from 3 to 7 dpf. We saw no differences in the position, timing or extent of *col2a1* expression between mutants and their siblings at 3 dpf, suggesting that the loss of *col11a2* has no impact on the expression of *col2a1a*, although alterations to craniofacial skeletal shape in the mutant were detectable from 5 dpf (electronic supplementary material, figure S2). We next used immunostaining to detect type II collagen protein in mutant and wt larvae. At 3 dpf, we could not detect any differences between wt and mutant larvae (figure 1*a*,*b*). However, by 5 dpf, clear differences in the distribution of type II collagen were seen in the lower jaw (denoted by asterisks in figure 1*a*,*b*). In wt fish, type II collagen can be seen in the ECM surrounding each chondrocyte in the lower-jaw cartilages, whereas in mutants, protein expression is

concentrated in the perichondrium and reduced between chondrocytes (dashed insets in figure 1*b*). Alongside this reduction in type II collagen in the more mature matrix towards the middle of the cartilage elements, small pieces of immunostained material were seen separate from the main elements (red asterisks in figure 1*b*) and ectopic expression of type II collagen in the ligament was observed (red arrow in figure 1*b*). Changes to the shape and size of the cartilage elements also became apparent at 5 dpf, with mutant larvae displaying thicker, shorter cartilage structures, with less definition. At 7 dpf, these shape discrepancies were maintained. A pronounced reduction and disorganization of type II collagen became clear by 7 dpf (figure 1*b*) and was more obvious in the cartilages that make up the lower jaw, with the lateral cartilage of the ear more preserved (figure 1*a*,*b*). Taken together, these data suggest that expression and synthesis of *col2a1a* are unaffected by loss of *col11a2*, but that maintenance of type II collagen protein is impaired in the mutants.

(c) Zebrafish with a *col11a2* mutation have altered jaw and joint morphology during development

Humans carrying mutations in type XI collagen show alterations to craniofacial shape, including midface hypoplasia and micrognathia [47,48]. From type II collagen immunostaining and Alizarin red/Alcian blue staining, we observed that mutant zebrafish also show altered craniofacial morphology (figures 1*b* and 3*d*). At 3 dpf, there was no significant difference in jaw morphology, but at 5 and 7 dpf, mutants had significantly shortened, wider jaws (figure 2*a*,*b*), in line with the broader, flatter face shape observed in patients with Stickler syndrome.

As people with mutations in type XI collagens also display abnormal joint shape [49] and increased susceptibility to OA [8], we generated 3D surface models of the joint between the Meckel's cartilage and the palatoquadrate (jaw joint) at 3, 5 and 7 dpf in wt and mutants (figure 2*c*,*d*). At 3 dpf, there was no significant change to joint morphology; however, at 5 and 7 dpf, mutants show enlarged terminal regions of the skeletal rudiments. Specifically, these changes were seen at the Meckel's cartilage neck and head adjacent to the joint (figure 2*e*,*f*, position of measurements shown by red and green lines in figure 2*c*). A reduction in the joint space (figure 2*g*, position of measurement shown by white line in figure 2*c*), such that the interzone is no longer clearly defined in the renders was also observed, probably due to the increased local deposition of type II collagen (figures 1*b* and 2*d*). These results show that the abnormal pattern of type II collagen deposition seen in *col11a2* zebrafish mutants at 5 and 7 dpf leads to altered joint shape.

(d) Mutation of *col11a2* leads to altered chondrocyte cell behaviour

Using confocal imaging of a transgenic reporter for *col2a1a*, we were also able to observe alterations to chondrocyte behaviour in mutant fish at 7 dpf. In wt larvae, all cells expressing *col2a1a* are located within the cartilage element; however, in mutants, we frequently observed chondrocytes located outside the main body of the cartilage element (figure 2*h*). We quantified the number of these cells in the lower-jaw cartilages of wt and mutant larvae during early development. Prior to 5 dpf, these spurs, which resemble hereditary multiple exostoses [50], are not observed (figure 2*i*). However, at 5 and 7 dpf, they are present in the Meckel's cartilage and ceratohyal of *col11a2* mutants, suggesting a failure of chondrocyte progenitor cells to fully intercalate into the cartilage element prior to expression of *col2a1a*.

In addition to these protrusions, we observed differences to chondrocyte morphology within the jaw elements of mutants at 5 dpf. Chondrocyte circularity is a measure of maturation, as in zebrafish chondrocytes become less rounded over time and form tightly packed stacks as they mature towards hypertrophy and show organization reminiscent of the mammalian cartilage growth plate. Chondrocytes in the centre of cartilage elements (representing the most mature chondrocytes) of *col11a2* mutants show increased circularity over those in wt cartilage (figure 2*j*). These results suggest that the maturation of chondrocytes in *col11a2* mutants is disrupted, potentially due to the loss of type II collagen from the ECM, which could provide an explanation for the thicker appearance of the cartilage elements in mutants.

(e) Larval and adult *col11a2* mutant zebrafish have altered material properties in the craniofacial skeleton

To test whether the loss of type II collagen and alterations to chondrocyte behaviour led to changes to the material properties of the cartilage, we performed AFM on dissected lower-jaw cartilages from 7 dpf wt and mutants. We tested the properties in regions containing immature cells close to the jaw joint and Meckel's symphysis (figure 3*a*) and observed a significant increase in YM from an average of 4.15–7.4 MPa (figure 3*b*). In more mature, intercalated cells towards the centre of the Meckel's cartilage (in which we saw loss of type II collagen), the difference in YM was around four times greater than that of comparable regions in wt (figure 3*b*). This suggests that the loss of type II collagen as a result of the *col11a2* mutation leads to stiffening of the cartilage ECM. As we observed altered material properties in larvae at pre-skeletonized stages, we wanted to test whether this would persist to adulthood and impact bone properties. We dissected jaw bones and operculae from wt and mutant fish and used AFM to establish YM. As in the larval cartilage, we observed that the bone from *col11a2* mutant fish had a significantly higher YM than siblings (figure 3*c*).

(f) Type II collagen loss is not accompanied by changes to glycosaminoglycans, type X or type I collagen in *col11a2* mutant zebrafish

As type II collagen was prematurely lost from maturing chondrocytes, we sought to examine whether GAGs were similarly reduced. We stained wt and mutant larvae with Alcian blue (to mark cartilage GAGs) and Alizarin red (to mark bone) at 5 and 7 dpf. We saw no reduction in GAG reactivity in the mutants at 5 or 7 dpf (figure 3*d*). Additionally, we saw no dramatic changes to Alizarin red, with dermal and chondral bones in mutants mineralizing at a similar rate to wt fish.

During cartilage maturation, a change in collagens from type II to type X collagen is associated with chondrocyte

hypertrophy [51]. In teleosts such as zebrafish, *col10a1a* marks hypertrophic chondrocytes, but also osteoblasts and ligament cells [52,53]. To test whether there was any change to the extent of chondrocyte hypertrophy or to the number of osteoblasts or skeletal connective tissue cells, we crossed the *col11a2* mutant into the *col10a1a* transgenic reporter (figure 3*e*). Quantification of *col10a1a*-positive cells in wt and mutant fish revealed no differences to the number of hypertrophic chondrocytes at 7 dpf (figure 3*f*, green arrows and graphs figure 3*g*,*h*), we also saw no difference in the number of osteoblasts in the dentary which is located directly adjacent to the MC (red arrows in figure 3*f*, quantification in figure 3*g*) or to the number of cells in the IOM ligament (purple arrows in figure 3*f*, quantification in figure 3*g*). This suggests that the onset of hypertrophy is not disrupted in *col11a2* fish, despite the 'less mature' appearance of their chondrocytes.

During cartilage degeneration, such as in OA, a switch of collagens is commonly reported with a reduction in type II and increase in type I collagen, associated with stiffer matrix [54]. To test whether loss of type II collagen led to replacement with type I, we performed immunostaining in wt and mutant larvae at 5 and 7 dpf. In wt fish, type I collagen was present in the jaw joint space, Meckel's symphysis and at a low level in the cartilage ECM, this pattern was unchanged in mutants at 5 dpf; however by 7 dpf, there was a reduction in type I collagen in the joint interzone of mutants but no change within the cartilage elements themselves (electronic supplementary material, figure S4).

Taken together, these results suggest that loss of type II collagen in *col11a2* mutants does not lead to loss of GAG, nor to compensatory increases of Col I or *col10a1*, and that hypertrophy is unaffected by the *col11a2* mutation. As a result, the increase in cartilage stiffness observed from AFM cannot be attributed to alterations in these components.

(g) Both shape and material properties impact the biomechanical performance of the zebrafish lower jaw

We have previously modelled the biomechanics of zebrafish jaw opening and closure during early ontogeny using finite element analysis (FEA) [43] and shown that paralysis and the accompanying changes to joint shape impact the strain pattern in the developing joint [33]. Therefore, we used FEA to model how the changes to shape and material properties observed in *col11a2* mutants would affect the biomechanical performance of the lower jaw. Meshes were generated of wt and mutant larvae at 7 dpf (meshes shown in electronic supplementary material, figure S5*b*). We applied muscle forces as per Roddy *et al*. [55] and used the material properties established from AFM (figure 3*b*).

We first modelled the wt and the mutant jaw shapes using the material properties established from each genotype and modelled a two-step process for jaw movement with step 1 denoting jaw closure and step 2 jaw opening (as per [43,55]) and visualized the maximum principal (E_{Max}) and minimum principal (E_{Min}) strains for jaw opening (figure 4) and closure (electronic supplementary material, figure S6). In the wt model, tensional strains (E_{Max}) are located laterally around the joint and either side of the Meckel's symphysis, focused on the muscle insertion points with the strain spreading widely through the element. By contrast, in mutants, maximum principal strain is concentrated on the joint interzone, with little spread through the cartilaginous element (note blue colour throughout the cartilage of mutants, cf. greens and yellows in wt) (figure 4*a*; electronic supplementary material, videos S1 and S2). Comparison of the Meckel's symphysis joint interzones for strains (E_{Max}) showed that the difference between the types of models (wt models and the mutant models) was far larger than the difference between each type of model with different material properties (electronic supplementary material, figure S5*c*,*d*). In the mutant model with mutant values, the joints averaged 1.63×10^{-2} maximum strains (E_{Max}), and in the mutant model with wt values, the joint strain averaged 1.51×10^{-2}, whereas in the wt models, the joint strains averaged 4.41×10^{-2} (E_{Max}) in the wt with wt values model, and 5.14×10^{-6} in the wt with mutant values model. Between each type of model (wt against mutant), the average maximum principal strains have not changed substantially, despite change in material properties. In wt, compressional strains (E_{Min}) are at the Meckel's symphysis, the medial surface of the anterior MC and on the dorsolateral side of the jaw joint (figure 4*a*; electronic supplementary material, figure 6*a*). In mutants, again, the minimum principal strains are more focal than in wt larvae (figure 4*a*; electronic supplementary material, figure S6*a*).

Changing the material properties of the models affects patterns of strain and displacement. This influences the displacement on the overall jaw morphology as seen in the jaw opening stage when both models are given the stiffer mutant material properties. In these models, the jaw shows less displacement in the opening movement compared to the situation in which models are given the less stiff wt material property values.

To test whether the change to the strain pattern was predominantly caused by the alteration to the shape of the jaw elements or the changes to YM, we next modelled the effect of mutant properties in the wt shape, and wt properties in the mutant shape (figure 4*b*; electronic supplementary material, figure S6*b*). We observed that changing YM in the wt shape to the mutant values decreased the spread of max and min principal strains, such that the pattern was intermediate between the mutant and wt. Likewise, inserting the wt values for cartilage into the mutant shape led to an increase in the extent of both tension (E_{Max}) and compression (E_{Min}). However, it did not fully 'rescue' the pattern, leading us to conclude that while both shape and material properties play a role in the mechanical performance of the tissue, the effect of shape is greater than that of material properties.

(h) *Col11a2* zebrafish mutants show impaired jaw function

As patients with Stickler syndrome suffer from joint hypermobility [56], and as *col11a2* zebrafish mutants show aberrant joint morphology, we looked at jaw function at 5 dpf. Zebrafish have two joints within the lower jaw and make distinct movements for feeding and breathing [57]. By filming and quantifying jaw movement, we observed that mutants make significantly fewer total movements than wt (figure 5*b*; electronic supplementary material, videos S3 and S4). This was due to a reduction in the number of movements involving the jaw joint, as we

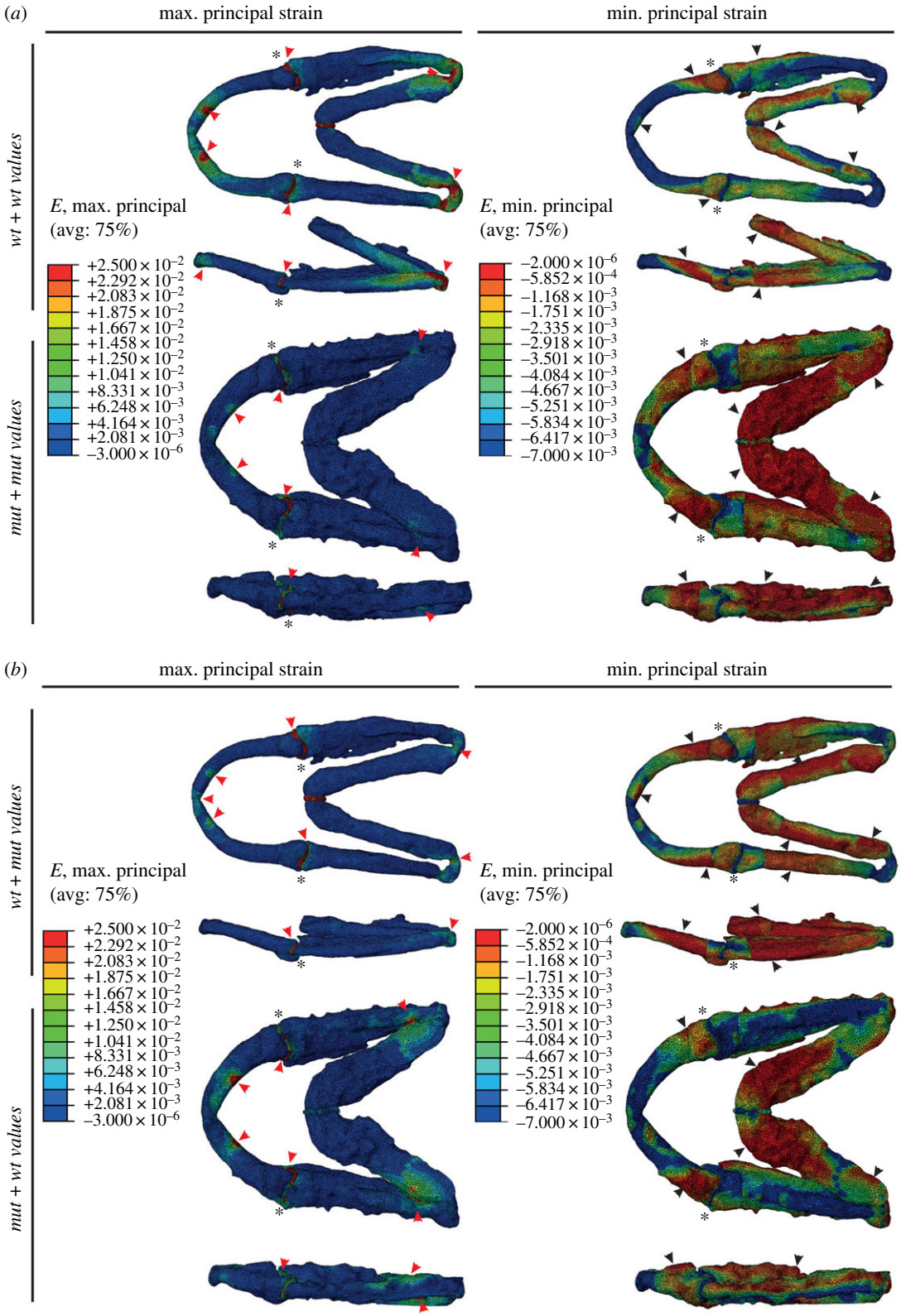

Figure 4. Shape changes in *col11a2* zebrafish mutants have a greater effect on jaw biomechanics than material property changes. (*a*,*b*) FE models of maximum (E_{Max}) and minimum (E_{Min}) principal strain during mouth opening in 7 dpf wt and *col11a2*−/− zebrafish. Red arrowheads, areas of high strain; black arrowheads, areas of low strain; black asterisks, jaw joint. (*a*) wt jaw shape with wt material properties and *col11a2*−/− shape with *col11a2*−/− material properties. (*b*) wt shape with *col11a2*−/− material properties and *col11a2*−/− shape with wt material properties. Ventral and lateral views shown for each condition.

observed no significant difference in the frequency of movements involving the buccal joint (figure 5*b*). However, mutant zebrafish show an increased range of motion at the buccal joint, which appears to dislocate (figure 5*a*,*c*). To rule out the possibility that this change to movement was caused by altered muscle patterning, we quantified the number of slow twitch fibres in the jaw at 5 dpf and saw no difference in fibre number between wt and mutants (electronic supplementary material, figure S7*a*,*b*). We also measured the diameter of the intermandibularis posterior and interhyoideus muscles in the lower jaw from birefringence and found no change in diameter between wt and mutants (electronic supplementary material, figure S7*c*). Taken together, this suggests that the alterations to joint

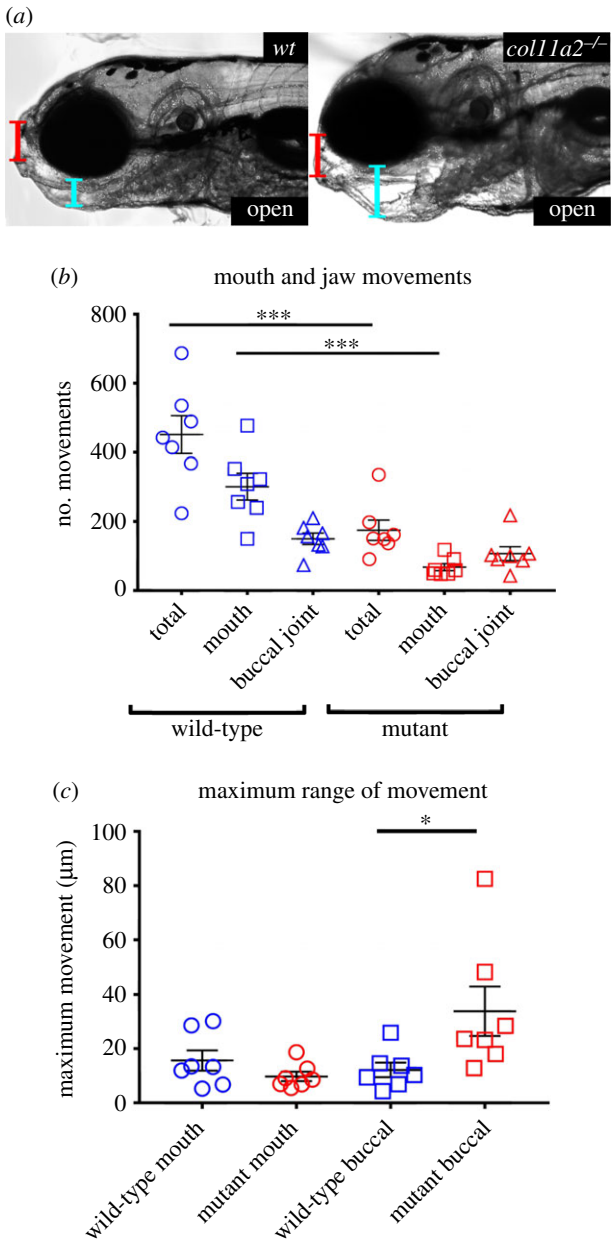

Figure 5. *col11a2* mutant zebrafish have abnormal jaw movement at 5 dpf. (*a*) Stills from high-speed movies show range of jaw movement in wt and *col11a2*−/−. (*b*,*c*) Analysis of (*b*) total jaw movements and (*c*) range of movement at two locations shown in (*a*): red line, mouth; blue line, buccal joint ($n = 7$ for all). Student's unpaired *t*-tests performed for *b* and *c*, data are mean with SEM. *$p \leq 0.05$, ***$p \leq 0.001$.

shape observed in *col11a2* mutants are the cause of abnormal joint function.

(i) Premature osteoarthritis is observed in adult *col11a2* heterozygous fish

Owing to the abnormalities in joint shape, mechanical performance and function in mutants, and because aberrant joint loading is highly associated with OA risk [58], we wanted to test whether adult mutants would develop premature OA. To address this question, we analysed 1-year-old heterozygous fish (*col11a2*+/−) and wt siblings using µCT. Craniofacial abnormalities were observed in *col11a2*+/−, including jaw protrusion and hypoplasia of the fronto-nasal bone (figure 6*a*). Changes in joint shape were observed in *col11a2*+/− accompanied by narrowing of the inter-joint space (figure 6*b*). To identify the histopathological changes related to OA, we stained wt and *col11a2*+/− joint sections for Alcian blue and H&E (figure 6*c*). While in wt sections, a defined cartilaginous layer lines the joint, in *col11a2*+/−, the cartilage shows signs of degradation. Grading of 5 sections per joint per fish ($n = 3$ fish) using the criteria in the OARSI scoring system [44] showed an average score of 6 in the *col11a2*+/− sections which is characterized by deformation and change in the contour of the articular surface, compared to an intact surface and normal cartilage with an average score of 0 in the siblings (figure 6*c*). Osteophytes were not observed. We analysed collagen organization using PicroSirius red staining and SHG (figure 6*d*,*e*). In wt jaws, the cartilaginous layer at the joint shows organized collagen fibres with a distinct orientation from those of the underlying bone (figure 6*d*, note change in colour from red to green in PicroSirius red staining). However, in the *col11a2*+/−, the transition from cartilage to bone is lost and the overall organization is perturbed (figure 6*d*). Thicker collagen bundles and fibres displaying abnormal orientations were seen through SHG in *col11a2*+/− samples (figure 6*e*). Taken together, these data demonstrate that loss of *col11a2* leads to early onset of OA-like changes in adults.

4. Discussion

Mutations in the type XI collagen genes *col11a1* and *col11a2* have previously been linked to numerous skeletal dysplasias, such as Stickler syndrome and fibrochondrogenesis, which are associated with cartilage destabilization, and abnormal skeletal shape and properties. Here, we describe the impact of loss of *col11a2* in zebrafish and show changes to ECM composition, material properties, craniofacial shape, mechanical performance, chondrocyte behaviour, and joint function in larval and adult fish.

Type XI collagen is important for the protection of type II collagen from degradation [46]; our data suggest that while transcription and secretion of type II collagen is unaffected at early stages of larval development, the assembly of type II collagen fibrils may be altered in mutants, making them more susceptible to degradation. This idea is given weight by the identification of fragments of type II-positive material seen surrounding the cartilage elements. What happens to those degraded collagen fragments is still unclear. Potentially, they may be cleared by the phagocytic cells of the innate immune system either with a rapid resolution or, alternatively, continued accumulation of these fragments could lead to the low-level inflammation associated with OA [59,60]. The loss or breakdown of type II collagen also occurs as the chondrocytes mature, such that the matrix between the chondrocytes almost completely lacks type II collagen, while the matrix of the perichondrium is relatively preserved. We have tested effects of *col11a2* loss on the material properties of cartilage and bone, and our data show an increase in YM in both tissues, with the greatest difference seen in mature chondrocytes. It may be noted that YM for zebrafish cartilage is higher than that from other species (4.15 MPa in fish versus 0.45 Mpa in human articular cartilage [61]). One likely explanation is the variation in relative ratio of cells to matrix during development and across species in evolution. In mature human articular

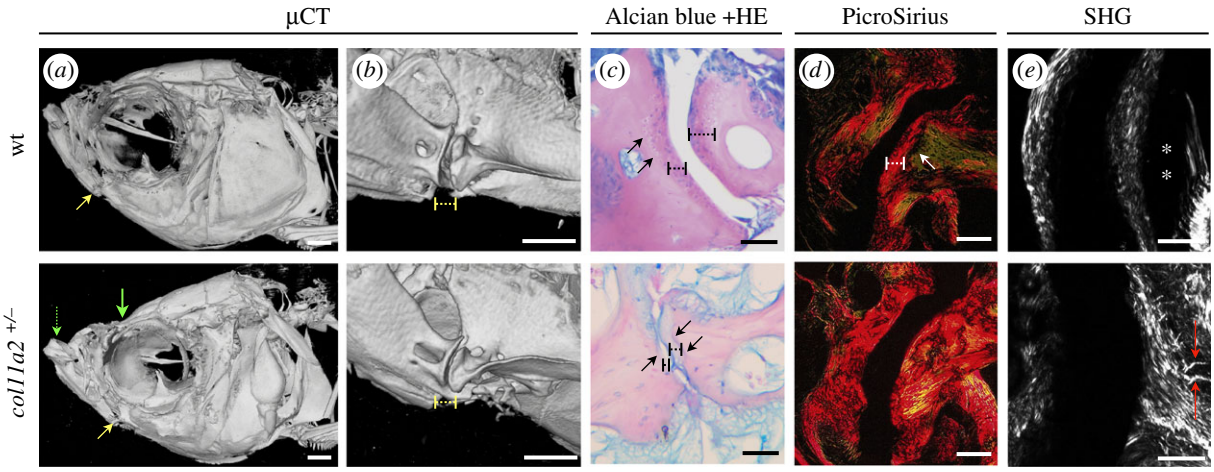

Figure 6. Mutations in zebrafish *col11a2* result in changes that trigger premature OA. (*a*,*b*) Three-dimensional renders from µCTs of 1-year-old wt and *col11a2* heterozygous mutant (*col11a2*+/−). (*a*) Yellow arrow, jaw joint; dashed green arrow, region of jaw protrusion in *col11a2*+/−; green arrow, region of hypoplasia in fronto-nasal skeleton. (*b*) Higher magnification image of joint region where dashed yellow line, inter-joint space. (*c*,*d*) Paraffin sections of the jaw joint stained with (*c*) Alcian blue and haematoxylin/eosin and (*d*) PicroSirius red. Dashed black line, cartilage layer; black arrows, underlying bone; dashed white line, cartilage; white arrow, bone (green). (*e*) SHG, asterisks pointing to areas of thinner fibres not detected by SHG, red arrows, thicker collagen bundles on abnormal orientation. Scale bars, 50 µm.

cartilage, the ratio is approximately 10 : 90 cells to matrix compared to 80 : 20 in zebrafish [62]. The higher YM in mutants was not explained by any obvious increased calcification, accumulation of type X or type I collagen or loss of GAG. In rodent models, increased matrix stiffness has been described as chondrocytes mature in the growth plate [63,64]. The stiffness of collagen matrix is controlled by several factors including fibre diameter and the density of intra-fibrillar cross-links, and abnormalities in collagen fibrillar assembly have been related to changes to mechanical properties of the cartilage during progression of OA [65] and ageing [66].

It has previously been reported that patients with Stickler syndrome develop premature OA (1), but the mechanism by which this occurs is unclear. We and others have previously shown that despite living in an aquatic environment, zebrafish can also develop alterations to the joint that strongly resemble OA [32,67]. Interestingly, we see premature development of OA in *col11a2* heterozygous adult zebrafish. This is manifested by abnormal collagen organization, degeneration of joint cartilage and loss of joint space. During OA, proteoglycans are lost from the cartilage prior to the degradation of the collagen network in the ECM (2). This change to the organization and content of collagen in the cartilage leads to changes in its material properties (3), including its stiffness and tensile strength (4). It has previously been demonstrated that in OA, cartilage stiffness is often reduced [17,68] while we saw a dramatic increase in cartilage matrix stiffness in the *col11a2* mutants, these measurements were taken from larvae. We saw increased YM in adult bone, both of dermal (operculum) and chondral (jaw) bone, albeit less dramatically than in the cartilage. Potentially, stiffer bone could exacerbate OA pathogenesis; as subchondral bone thickening accelerates the degradation of articular cartilage [69]. Alternatively, and perhaps more likely, changes to joint loading from the abnormal shape and function throughout life may be the driver for the development of pathogenic OA-like changes in the joint. To test this more fully, it would be desirable to follow the development of the pathology throughout the life course of the fish.

As joint mechanical performance is impacted by its shape and the material properties of the tissues, we explored the relative impact of each by testing the impact of altering material properties in the wt and mutant shapes. From this, we deduced that while both contribute to the strain pattern, the larger impact comes from joint architecture. However, questions remain to the exact sequence of events; are the increases in YM in immature chondrocytes sufficient to drive local changes to cell behaviour within the joint? If so, subtle changes to joint morphology could impact joint mechanics upon onset of function, leading to further, more significant changes to skeletal cell behaviour. Movement of joints has been shown to be required for their correct specification in the majority of joint types in all species studied [26,70–73]. Interestingly, at the earliest stages we studied (3 dpf), prior to the onset of joint movement, the mutants are barely distinguishable from wts, despite the *col11a2* gene being expressed throughout the cartilage from 2 dpf. Following the onset of movement changes between wt and mutants become more pronounced, these include the degradation of type II collagen from the mature matrix, and the loss of the joint space. This loss of correct joint spacing and the enlargement of the rudiments could be explained by premature differentiation of the immature cells of the interzone. A requirement for normal movement has been demonstrated in chick, mouse and fish to maintain joint space and to prevent ectopic expression of type II collagen [33,34,74,75]. Alternatively, it could represent a failure to maintain local gdf5 signalling; it has recently been shown that there is a requirement for the continued influx of Gdf5-positive cells for correct joint specification [76].

It is likely that by changing the mechanical performance of the joint, mechanosensitive genes will be differentially activated, and these probably control the cellular changes we describe. Candidates that could be differentially activated in the mutants could include the Piezo ion channels, which have been shown to play a role in OA [77]. Another candidate could be the YAP pathway—YAP is implicated in negative control of chondrogenesis [78,79]—or the genes in the Wnt signalling pathway. The Wnt pathway has been implicated

in developmental skeletal mechanosensation in mice, chicks [80] and zebrafish [81], and could potentially be acting in combination with BMP regulatory genes such as Smurf1 [82]. We have shown in zebrafish that wnt16 controls chondrocyte proliferation and migration in the joint region. Wnt16 is also linked to hip geometry [83], altered cortical bone thickness [84,85], the response of chondrocytes to injury and to OA [86,87].

Following the onset of movement, we also see the appearance of cells located outside the cartilage anlage, which bear some resemblance to multiple hereditary exostoses (MHE). Stickler syndrome is associated with MHEs [10]. It has been reported in a zebrafish model that the development of MHE is driven by changes to the matrix from loss of the Extosin genes, which, while dispensable for early chondrocyte differentiation are required for chondrocyte maturation, hypertrophy and intercalation, and which encode genes lead to matrix sulfation [50]. Potentially, the loss of type II collagen in the *col11a2* mutants could perturb sulfation. Alternatively, these cells could fail to intercalate, then be extruded due to altered joint function, as paralysis has been shown to control chondrocyte intercalation in zebrafish [88]. The failure of these cells to fully intercalate leads to shorter, thicker elements in *col11a2* mutants.

Taken together, our findings show that loss of *col11a2* in zebrafish leads to changes to matrix phenotype, and cell behaviour that impacts the biomechanical and functional performance of the developing joint, leading to premature OA. By making use of the detailed dynamic imaging unique to small translucent models like the zebrafish, we were able to follow the alterations to the developing skeleton at cellular resolution, identifying changes to cell behaviour that go some way to explaining how loss of a relatively minor collagen subtype can have such a profound effect on the human skeleton in diseases such as Stickler syndrome and fibrochondrogenesis.

Data accessibility. This article has no additional data.

Author's contributions. E.A.L., K.A.R. and E.K. carried out the molecular laboratory work, participated in data analysis, participated in the design of the study and drafted the manuscript; J.A.A. generated the FE models; R.L.H. performed AFM; C.L.H. conceived the study, designed the study, coordinated the study and helped draft the manuscript. All authors gave final approval for publication.

Competing interests. The authors declare no competing interests.

Funding. C.L.H. and E.K. were funded by Arthritis Research UK grants 21211 and 19947. K.A.R. was funded by the MRC (MR/L002566/1). E.A.L. is funded by a Wellcome Trust Dynamic Molecular Cell Biology PhD programme. PeakForce AFM was carried with equipment funded by the EPSRC (EP/K035746/1).

Acknowledgements. The authors would like to thank Stephen Cross and the Wolfson Biomaging facility staff for help with image acquisition and analysis.

References

1. Weiss C, Rosenberg L, Helfet AJ. 1968 An ultrastructural study of normal young adult human articular cartilage. *J. Bone Joint Surg. Am.* **50**, 663–674. (doi:10.2106/00004623-196850040-00002)
2. Vaughan L, Mendler M, Huber S, Bruckner P, Winterhalter K, Irwin M, Mayne R. 1988 D-periodic distribution of collagen IX along cartilage fibrils. *J. Cell Biol.* **106**, 991–997. (doi:10.1083/jcb.106.3.991)
3. Mendler M, Eich-Bender SG, Vaughan L, Winterhalter KH, Bruckner P. 1989 Cartilage contains mixed fibrils of collagen types II, IX, and XI. *J. Cell Biol.* **108**, 191–197. (doi:10.1083/jcb.108.1.191)
4. Fox AJS, Bedi A, Rodeo SA. 2009 The basic science of articular cartilage: structure, composition, and function. *Sports Health* **1**, 461. (doi:10.1177/1941738109350438)
5. Burgeson RE, Hollister DW. 1979 Collagen heterogeneity in human cartilage: identification of several new collagen chains. *Biochem. Biophys. Res. Commun.* **87**, 1124–1131. (doi:10.1016/S0006-291X(79)80024-8)
6. Eyre DR. 1991 The collagens of articular cartilage. *Semin. Arthritis Rheum.* **21**, 2–11. (doi:10.1016/0049-0172(91)90035-X)
7. Hafez A, Squires R, Pedracini A, Joshi A, Seegmiller RE, Oxford JT. 2015 Col11a1 regulates bone microarchitecture during embryonic development. *J. Dev. Biol.* **3**, 158. (doi:10.3390/jdb3040158)
8. Couchouron T, Masson C. 2011 Early-onset progressive osteoarthritis with hereditary progressive ophthalmopathy or Stickler syndrome. *Jt. Bone Spine* **78**, 45–49. (doi:10.1016/j.jbspin.2010.03.012)
9. Vikkula M *et al.* 1995 Autosomal dominant and recessive osteochondrodysplasias associated with the COL11A2 locus. *Cell* **80**, 431–437. (doi:10.1016/0092-8674(95)90493-X)
10. Sirko-Osadsa DA, Murray MA, Scott JA, Lavery MA, Warman ML, Robin NH. 1998 Stickler syndrome without eye involvement is caused by mutations in COL11A2, the gene encoding the α2(XI) chain of type XI collagen. *J. Pediatr.* **132**, 368–371. (doi:10.1016/S0022-3476(98)70466-4)
11. Acke FR *et al.* 2014 Novel pathogenic COL11A1/COL11A2 variants in Stickler syndrome detected by targeted NGS and exome sequencing. *Mol. Genet. Metab.* **113**, 230–235. (doi:10.1016/j.ymgme.2014.09.001)
12. Kuivaniemi H, Tromp G, Prockop DJ. 1991 Genetic causes of aortic aneurysms. Unlearning at least part of what the textbooks say. *J. Clin. Invest.* **88**, 1441. (doi:10.1172/JCI115452)
13. Tompson SW *et al.* 2012 Dominant and recessive forms of fibrochondrogenesis resulting from mutations at a second locus, COL11A2. *Am. J. Med. Genet. A* **158A**, 309–314. (doi:10.1002/ajmg.a.34406)
14. Seegmiller RE, Fraser FC, Sheldon H. 1971 A new chondrodystrophic mutant in mice. *J. Cell Biol.* **48**, 580–593. (doi:10.1083/jcb.48.3.580)
15. Fernandes RJ, Weis M, Scott MA, Seegmiller RE, Eyre DR. 2007 Collagen XI chain misassembly in cartilage of the chondrodysplasia (cho) mouse. *Matrix. Biol.* **26**, 597–603. (doi:10.1016/j.matbio.2007.06.007)
16. Rodriguez RR, Seegmiller RE, Stark MR, Bridgewater LC. 2004 A type XI collagen mutation leads to increased degradation of type II collagen in articular cartilage. *Osteoarthr. Cartil.* **12**, 314–320. (doi:10.1016/j.joca.2003.12.002)
17. Xu L, Flahiff CM, Waldman BA, Wu D, Olsen BR, Setton LA, Li Y. 2003 Osteoarthritis-like changes and decreased mechanical function of articular cartilage in the joints of mice with the chondrodysplasia gene (cho). *Arthritis Rheum.* **48**, 2509–2518. (doi:10.1002/art.11233)
18. Holyoak DT *et al.* 2017 Collagen XI mutation lowers susceptibility to load-induced cartilage damage in mice. *J. Orthop. Res.* **36**, 711–720. (doi:10.1002/jor.23731)
19. McGuirt WT *et al.* 1999 Mutations in COL11A2 cause non-syndromic hearing loss (DFNA13). *Nat. Genet.* **23**, 413–419. (doi:10.1038/70516)
20. Luo YY. 2016 Type XI collagen. In *Biochemistry of collagens, laminins and elastin* (ed. MA Karsdal), pp. 77–80. New York: Academic Press.
21. Chen Y, Chen M, Gaffney EA, Brown CP. 2017 Effect of crosslinking in cartilage-like collagen microstructures. *J. Mech. Behav. Biomed. Mater.* **66**, 138–143. (doi:10.1016/j.jmbbm.2016.10.006)
22. Radlanski RJ, Renz H. 2006 Genes, forces, and forms: mechanical aspects of prenatal craniofacial development. *Dev. Dyn.* **235**, 1219–1229. (doi:10.1002/dvdy.20704)

23. Alexopoulos LG, Haider MA, Vail TP, Guilak F. 2003 Alterations in the mechanical properties of the human chondrocyte pericellular matrix with osteoarthritis. *J. Biomech. Eng.* **125**, 323–333. (doi:10.1115/1.1579047)
24. Waarsing JH, Kloppenburg M, Slagboom PE, Kroon HM, Houwing-Duistermaat JJ, Weinans H, Meulenbelt I. 2011 Osteoarthritis susceptibility genes influence the association between hip morphology and osteoarthritis. *Arthritis Rheum.* **63**, 1349–1354. (doi:10.1002/art.30288)
25. Baird DA *et al*. 2018 Investigation of the relationship between susceptibility loci for hip osteoarthritis and DXA-derived hip shape in a population based cohort of peri-menopausal women. *Arthritis Rheumatol*.
26. Verbruggen SW, Kainz B, Shelmerdine SC, Hajnal JV., Rutherford MA, Arthurs OJ, Phillips AT, Nowlan NC. 2018 Stresses and strains on the human fetal skeleton during development. *J. R. Soc. Interface* **15**, 20170593. (doi:10.1098/rsif.2017.0593)
27. Hammond CL, Moro E. 2012 Using transgenic reporters to visualize bone and cartilage signaling during development *in vivo*. *Front Endocrinol.* (*Lausanne*) **3**, 91. (doi:10.3389/fendo.2012.00091)
28. Witten PE, Harris MP, Huysseune A, Winkler C. 2017 Small teleost fish provide new insights into human skeletal diseases. In *Methods in cell biology* (eds HW Detrich III, M Westerfield, LI Zon), pp. 321–346. Cambridge MA, USA: Academic Press.
29. Eames B, DeLaurier A, Ullmann B, Huycke TR, Nichols JT, Dowd J, McFadden M, Sasaki MM, Kimmel CB. 2013 FishFace: interactive atlas of zebrafish craniofacial development at cellular resolution. *BMC Dev. Biol.* **13**, 23. (doi:10.1186/1471-213X-13-23)
30. Schilling TF, Le Pabic P. 2009 Fishing for the signals that pattern the face. *J. Biol.* **8**, 101. (doi:10.1186/jbiol205)
31. Askary A, Xu P, Barske L, Bay M, Bump P, Balczerski B, Bonaguidi MA, Crump JG. 2017 Genome-wide analysis of facial skeletal regionalization in zebrafish. *Development* **144**, 2994–3005. (doi:10.1242/dev.151712)
32. Askary A, Smeeton J, Paul S, Schindler S, Braasch I, Ellis NA, Postlethwait J, Miller CT, Crump JG. 2016 Ancient origin of lubricated joints in bony vertebrates. *Elife* 5, e16415.
33. Brunt LH, Skinner REH, Roddy KA, Araujo NM, Rayfield EJ, Hammond CL. 2016 Differential effects of altered patterns of movement and strain on joint cell behaviour and skeletal morphogenesis. *Osteoarthr. Cartil.* **24**, 1940–1950. (doi:10.1016/j.joca.2016.06.015)
34. Brunt LH, Norton JL, Bright JA, Rayfield EJ, Hammond CL. 2015 Finite element modelling predicts changes in joint shape and cell behaviour due to loss of muscle strain in jaw development. *J. Biomech.* **48**, 3112–3122. (doi:10.1016/j.jbiomech.2015.07.017)
35. Baas D, Malbouyres M, Haftek-Terreau Z, Le Guellec D, Ruggiero F. 2009 Craniofacial cartilage morphogenesis requires zebrafish col11a1 activity. *Matrix. Biol.* **28**, 490–502. (doi:10.1016/j.matbio.2009.07.004)
36. Westerfield M. 2000 *The zebrafish book: a guide for the laboratory use of zebrafish* (*Danio rerio*), 4th edn. Eugene, OR, USA: University of Oregon Press.
37. Hammond CL, Schulte-Merker S. 2009 Two populations of endochondral osteoblasts with differential sensitivity to Hedgehog signalling. *Development* **136**, 3991–4000. (doi:10.1242/dev.042150)
38. Elworthy S, Hargrave M, Knight R, Mebus K, Ingham PW. 2008 Expression of multiple slow myosin heavy chain genes reveals a diversity of zebrafish slow twitch muscle fibres with differing requirements for Hedgehog and Prdm1 activity. *Development* **135**, 2115–2126. (doi:10.1242/dev.015719)
39. Schindelin J *et al.* 2012 Fiji: an open-source platform for biological-image analysis. *Nat. Methods* **9**, 676–682. (doi:10.1038/nmeth.2019)
40. Walker M, Kimmel C. 2007 A two-color acid-free cartilage and bone stain for zebrafish larvae. *Biotech. Histochem.* **82**, 23–28. (doi:10.1080/10520290701333558)
41. Thisse C, Thisse B. 2008 High-resolution in situ hybridization to whole-mount zebrafish embryos. *Nat. Protoc.* **3**, 59–69. (doi:10.1038/nprot.2007.514)
42. Fang M, Adams JS, McMahan BL, Brown RJ, Oxford JT. 2010 The expression patterns of minor fibrillar collagens during development in zebrafish. *Gene Expr. Patterns* **10**, 315–322. (doi:10.1016/j.gep.2010.07.002)
43. Brunt LH, Roddy KA, Rayfield EJ, Hammond CL. 2016 Building finite element models to investigate zebrafish jaw biomechanics video link. *J. Vis. Exp.* 54811.
44. Glasson SS, Chambers MG, Van Den Berg WB, Little CB. 2010 The OARSI histopathology initiative—recommendations for histological assessments of osteoarthritis in the mouse. *Osteoarthr. Cartil.* **18**, S17–S23. (doi:10.1016/j.joca.2010.05.025)
45. Chen X, Nadiarynkh O, Plotnikov S, Campagnola PJ. 2012 Second harmonic generation microscopy for quantitative analysis of collagen fibrillar structure. *Nat. Protoc.* **7**, 654–669. (doi:10.1038/nprot.2012.009)
46. Blaschke UK, Eikenberry EF, Hulmes DJ, Galla HJ, Bruckner P. 2000 Collagen XI nucleates self-assembly and limits lateral growth of cartilage fibrils. *J. Biol. Chem.* **275**, 10 370–10 378. (doi:10.1074/jbc.275.14.10370)
47. Robin NH, Moran RT, Ala-Kokko L. 1993 *Stickler syndrome. GeneReviews®*. Seattle, WA: University of Washington.
48. Hunt NCA, Vujani GM. 1998 Fibrochondrogenesis in a 17-week fetus: a case expanding the phenotype. *Am. J. Med. Genet.* **75**, 326–329. (doi:10.1002/(SICI)1096-8628(19980123)75:3<326::AID-AJMG20>3.0.CO;2-Q)
49. Randrianaivo H, Haddad G, Roman H, Lise A, Toutain A, Le Merrer M, Moraine C. 2002 Fetal fibrochondrogenesis at 26 weeks' gestation. *Prenat. Diagn.* **22**, 806–810. (doi:10.1002/pd.423)
50. Clément A, Wiweger M, von der Hardt S, Rusch MA, Selleck SB, Chien C-B, Roehl HH. 2008 Regulation of zebrafish skeletogenesis by *ext2/dackel* and *papst1/pinscher*. *PLoS Genet.* **4**, e1000136. (doi:10.1371/journal.pgen.1000136)
51. Schmid TM, Bonen DK, Luchene L, Linsenmayer TF. 1991 Late events in chondrocyte differentiation: hypertrophy, type X collagen synthesis and matrix calcification. *In Vivo* **5**, 533–540.
52. Eames BF, Amores A, Yan Y-L, Postlethwait JH. 2012 Evolution of the osteoblast: skeletogenesis in gar and zebrafish. *BMC Evol. Biol.* **12**, 27. (doi:10.1186/1471-2148-12-27)
53. Mitchell RE, Huitema LFA, Skinner REH, Brunt LH, Severn C, Schulte-Merker S, Hammond CL. 2013 New tools for studying osteoarthritis genetics in zebrafish. *Osteoarthr. Cartil.* **21**, 269–278. (doi:10.1016/j.joca.2012.11.004)
54. Miosge N, Hartmann M, Maelicke C, Herken R. 2004 Expression of collagen type I and type II in consecutive stages of human osteoarthritis. *Histochem. Cell Biol.* **122**, 229–236. (doi:10.1007/s00418-004-0697-6)
55. Roddy KA, Skinner RE, Brunt LH, Kague E, Cross S, Rayfield EJ, Hammond CL. 2017 A zebrafish model of developmental joint dysplasia: manipulating the larval 1 mechanical environment to drive the malformation and recovery of joint shape.
56. Stickler GB, Belau PG, Farrell FJ, Jones JD, Pugh DG, Steinberg AG *et al.* 1965 Hereditary progressive arthro-ophthalmopathy. *Mayo Clin. Proc.* **40**, 433–455.
57. Hernandez LP, Barresi MJF, Devoto SH. 2002 Functional morphology and developmental biology of zebrafish: reciprocal illumination from an unlikely couple. *Integr. Comp. Biol.* **42**, 222–231. (doi:10.1093/icb/42.2.222)
58. Buckwalter JA, Anderson DD, Brown TD, Tochigi Y, Martin JA. 2013 The roles of mechanical stresses in the pathogenesis of osteoarthritis: implications for treatment of joint injuries. *Cartilage* **4**, 286–294. (doi:10.1177/1947603513495889)
59. Scanzello CR, Goldring SR. 2012 The role of synovitis in osteoarthritis pathogenesis. *Bone* **51**, 249–257. (doi:10.1016/j.bone.2012.02.012)
60. Sokolove J, Lepus CM. 2013 Role of inflammation in the pathogenesis of osteoarthritis: latest findings and interpretations. *Ther. Adv. Musculoskelet. Dis.* **5**, 77–94. (doi:10.1177/1759720X12467868)
61. Mansour J. 2003 Biomechanics of cartilage. In *Kinesiology; the mechanics and pathomechanics of human movement* (ed. CA Oatis), pp. 1992–1996. Baltimore, MD: Lippincott Williams & Wilkins.
62. Hall BK, Brian K. 2015 *Bones and cartilage: developmental and evolutionary skeletal biology*. 892 p. Cambridge MA, USA: Academic Press.
63. Prein C, Warmbold N, Farkas Z, Schieker M, Aszodi A, Clausen-Schaumann H. 2016 Structural and mechanical properties of the proliferative zone of the developing murine growth plate cartilage

assessed by atomic force microscopy. *Matrix. Biol.* **50**, 1–15. (doi:10.1016/j.matbio.2015.10.001)
64. Radhakrishnan P, Lewis NT, Mao JJ. 2004 Zone-specific micromechanical properties of the extracellular matrices of growth plate cartilage. *Ann. Biomed. Eng.* **32**, 284–291. (doi:10.1023/B:ABME.0000012748.41851.b4)
65. Franz T, Hasler EM, Hagg R, Weiler C, Jakob RP, Mainil-Varlet P. 2001 *In situ* compressive stiffness, biochemical composition, and structural integrity of articular cartilage of the human knee joint. *Osteoarthr. Cartil.* **9**, 582–592. (doi:10.1053/joca.2001.0418)
66. Geraghty B, Jones SW, Rama P, Akhtar R, Elsheikh A. 2012 Age-related variations in the biomechanical properties of human sclera. *J. Mech. Behav. Biomed. Mater.* **16**, 181–191. (doi:10.1016/j.jmbbm.2012.10.011)
67. Hayes AJ, Reynolds S, Nowell MA, Meakin LB, Habicher J, Ledin J, Bashford A, Caterson B, Hammond CL. 2013 Spinal deformity in aged zebrafish is accompanied by degenerative changes to their vertebrae that resemble osteoarthritis. *PLoS ONE* **8**, e75787. (doi:10.1371/journal.pone.0075787)
68. Naveen SV, Ahmad RE, Hui WJ, Suhaeb AM, Murali MR, Shanmugam R, Kamarul T. 2014 Histology, glycosaminoglycan level and cartilage stiffness in monoiodoacetate-induced osteoarthritis: comparative analysis with anterior cruciate ligament transection in rat model and human osteoarthritis. *Int. J. Med. Sci.* **11**, 97–105. (doi:10.7150/ijms.6964)
69. Sharma AR, Jagga S, Lee S-S, Nam J-S. 2013 Interplay between cartilage and subchondral bone contributing to pathogenesis of osteoarthritis. *Int. J. Mol. Sci.* **14**, 19 805–19 830. (doi:10.3390/ijms141019805)
70. Pollard AS, Boyd S, McGonnell IM, Pitsillides AA. 2017 The role of embryo movement in the development of the furcula. *J. Anat.* **230**, 435–443. (doi:10.1111/joa.12571)
71. Pitsillides AA. 2006 Early effects of embryonic movement: 'a shot out of the dark'. *J. Anat.* **208**, 417–431. (doi:10.1111/j.1469-7580.2006.00556.x)
72. Rolfe RA, Bezer JH, Kim T, Zaidon AZ, Oyen ML, Iatridis JC, Nowlan NC. 2017 Abnormal fetal muscle forces result in defects in spinal curvature and alterations in vertebral segmentation and shape. *J. Orthop. Res.* **35**, 2135–2144. (doi:10.1002/jor.23518)
73. Nowlan NC, Chandaria V, Sharpe J. 2014 Immobilized chicks as a model system for early-onset developmental dysplasia of the hip. *J. Orthop. Res.* **32**, 777–785. (doi:10.1002/jor.22606)
74. Roddy KA, Prendergast PJ, Murphy P. 2011 Mechanical influences on morphogenesis of the knee joint revealed through morphological, molecular and computational analysis of immobilised embryos. *PLoS ONE* **6**, e17526. (doi:10.1371/journal.pone.0017526)
75. Kahn J *et al.* 2009 Muscle contraction is necessary to maintain joint progenitor cell fate. *Dev. Cell* **16**, 734–743. (doi:10.1016/j.devcel.2009.04.013)
76. Shwartz Y, Viukov S, Krief S, Zelzer E. 2016 Joint development involves a continuous influx of Gdf5-positive cells. *Cell Rep.* **15**, 2577–2587. (doi:10.1016/j.celrep.2016.05.055)
77. Lee W *et al.* 2014 Synergy between Piezo1 and Piezo2 channels confers high-strain mechanosensitivity to articular cartilage. *Proc. Natl Acad. Sci. USA* **111**, E5114–E5122. (doi:10.1073/pnas.1414298111)
78. Karystinou A, Roelofs AJ, Neve A, Cantatore FP, Wackerhage H, De Bari C. 2015 Yes-associated protein (YAP) is a negative regulator of chondrogenesis in mesenchymal stem cells. *Arthritis Res. Ther.* **17**, 147. (doi:10.1186/s13075-015-0639-9)
79. Deng Y, Wu A, Li P, Li G, Qin L, Song H, Mak KK. 2016 Yap1 regulates multiple steps of chondrocyte differentiation during skeletal development and bone repair. *Cell Rep.* **14**, 2224–2237. (doi:10.1016/j.celrep.2016.02.021)
80. Rolfe RA, Nowlan NC, Kenny EM, Cormican P, Morris DW, Prendergast PJ, Kelly D, Murphy P. 2014 Identification of mechanosensitive genes during skeletal development: alteration of genes associated with cytoskeletal rearrangement and cell signalling pathways. *BMC Genomics* **15**, 48. (doi:10.1186/1471-2164-15-48)
81. Brunt LH, Begg K, Kague E, Cross S, Hammond CL. 2017 Wnt signalling controls the response to mechanical loading during zebrafish joint development. *Development* **144**, 2798–2809. (doi:10.1242/dev.153528)
82. Singh PNP, Shea CA, Sonker SK, Rolfe RA, Ray A, Kumar S, Gupta P, Murphy P, Bandyopadhyay A. 2018 Precise spatial restriction of BMP signaling in developing joints is perturbed upon loss of embryo movement. *Development* **145**, dev153460. (doi:10.1242/dev.153460)
83. García-Ibarbia C, Pérez-Núñez MI, Olmos JM, Valero C, Pérez-Aguilar MD, Hernández JL, Zarrabeitia MT, Gonzalez-Macias J, Riancho JA. 2013 Missense polymorphisms of the WNT16 gene are associated with bone mass, hip geometry and fractures. *Osteoporos. Int.* **24**, 2449–2454. (doi:10.1007/s00198-013-2302-0)
84. Movérare-Skrtic S *et al.* 2014 Osteoblast-derived WNT16 represses osteoclastogenesis and prevents cortical bone fragility fractures. *Nat. Med.* **20**, 1279–1288. (doi:10.1038/nm.3654)
85. Ohlsson C *et al.* 2018 Inducible *Wnt16* inactivation: WNT16 regulates cortical bone thickness in adult mice. *J. Endocrinol.* **237**, 113–122. (doi:10.1530/JOE-18-0020)
86. Nalesso G *et al.* 2017 WNT16 antagonises excessive canonical WNT activation and protects cartilage in osteoarthritis. *Ann. Rheum. Dis.* **76**, 218–226. (doi:10.1136/annrheumdis-2015-208577)
87. Dell'Accio F, De Bari C, Eltawil NM, Vanhummelen P, Pitzalis C. 2008 Identification of the molecular response of articular cartilage to injury, by microarray screening: Wnt-16 expression and signaling after injury and in osteoarthritis. *Arthritis Rheum.* **58**, 1410–1421. (doi:10.1002/art.23444)
88. Shwartz Y, Farkas Z, Stern T, Aszódi A, Zelzer E. 2012 Muscle contraction controls skeletal morphogenesis through regulation of chondrocyte convergent extension. *Dev. Biol.* **370**, 154–163. (doi:10.1016/j.ydbio.2012.07.026)